Tidal Interaction between the UX Tauri A/C Disk System Revealed by ALMA

Luis A. Zapata[1] , Luis F. Rodríguez[1,2] , Manuel Fernández-López[3], Aina Palau[1] , Robert Estalella[4] , Mayra Osorio[5] ,
Guillem Anglada[5] , and Nuria Huelamo[6]

[1] Instituto de Radioastronomía y Astrofísica, Universidad Nacional Autónoma de México, P.O. Box 3-72, 58090, Morelia, Michoacán, México
l.zapata@irya.unam.mx

[2] Mesoamerican Centre for Theoretical Physics, Universidad Autónoma de Chiapas, Carretera Emiliano Zapata Km. 4 Real del Bosque, 29050 Tuxtla Gutiérrez, Chiapas, México

[3] Instituto Argentino de Radioastronomía (CCT-La Plata, CONICET; CICPBA), C.C. No. 5, 1894, Villa Elisa, Buenos Aires, Argentina

[4] Dep. de Física Quàntica i Astrofísica, Institut de Ciencies del Cosmos, Universitat de Barcelona, IEEC-UB, Marti i Franques 1, E-08028 Barcelona, Spain

[5] Instituto de Astrofísica de Andalucía(CSIC), Glorieta de la Astronomía s/n E-18008 Granada, Spain

[6] Centro de Astrobiología (CSIC-INTA), Camino bajo del Castillo s/n, E-28692 Villanueva de la Cañada, Madrid, Spain

Received 2020 January 31; revised 2020 May 1; accepted 2020 May 2; published 2020 June 19

Abstract

We present sensitive and high angular-resolution ($\sim$0.''2–0.''3) (sub)millimeter (230 and 345 GHz) continuum and CO(2−1)/CO(3−2) line archive observations of the disk star system in UX Tauri carried out with the Atacama Large Millimeter/Submillimeter Array. These observations reveal the gas and dusty disk surrounding the young star UX Tauri A with a large signal-to-noise ratio (>400 in the continuum and >50 in the line), and for the first time we detect the molecular gas emission associated with the disk of UX Tauri C (with a size for the disk of <56 au). No (sub)millimeter continuum emission is detected at the 5σ level (0.2 mJy at 0.85 mm) associated with UX Tauri C. For the component UX Tauri C, we estimate a dust disk mass of $\leqslant$0.05 $M_\oplus$. Additionally, we report a strong tidal disk interaction between both disks, UX Tauri A/C, separated 360 au in projected distance. The CO line observations reveal marked spiral arms in the disk of UX Tauri A and an extended redshifted stream of gas associated with the UX Tauri C disk. No spiral arms are observed in the dust continuum emission of UX Tauri A. Assuming a Keplerian rotation we estimate the enclosed masses (disk+star) from their radial velocities in $1.4 \pm 0.6\,M_\odot$ for UX Tauri A, and $70 \pm 30/\sin i$ Jupiter masses for UX Tauri C (the latter coincides with the mass upper limit value for a brown dwarf). The observational evidence presented here lead us to propose that UX Tauri C has a close approach of a possible wide, evolving, and eccentric orbit around the disk of UX Tauri A, causing the formation of spiral arms and a stream of molecular gas falling toward UX Tauri C.

1. Introduction

One of the natural consequences of the angular momentum conservation and energy dissipation in the formation of stars is circumstellar disks (Bate 2018). To date, dozens of circumstellar disks have been imaged employing different observational techniques. In the Orion Nebula Cloud, for example, many of these disks have been revealed through resolving the scattered light and silhouette images of disks using observations of the Hubble Space Telescope with an angular resolution of 0.''1 (Bally et al. 2000; O'Dell et al. 2008). Another key technique that is used for revealing disks is direct imaging of the centimeter, millimeter, and submillimeter thermal continuum and line emission utilizing the interferometric aperture synthesis technique (Williams & Cieza 2011; Osorio et al. 2016; Ansdell et al. 2017; Zapata et al. 2017; Huang et al. 2018; Kurtovic et al. 2018; Ruíz-Rodríguez et al. 2018; van der Plas et al. 2019). Some of these sensitive submillimeter observations have revealed possible encounters between close-by circumstellar disks (Dai et al. 2015; Kurtovic et al. 2018; Akiyama et al. 2019; van der Plas et al. 2019). The CO(2−1) line and 1.25 mm continuum emission revealed clear signatures of tidal interactions with spiral arms and extended stream-like emission in the disk system AS 205 (Kurtovic et al. 2018). Given that most of the stars are formed in binary or multiple systems (Duchêne & Kraus 2013), more cases of disk interaction might be revealed with more sensitive Atacama Large Millimeter/submillimeter Array (ALMA) observations.

There are a large number of works (e.g., Adams et al. 1989; Laughlin & Korchagin 1996) that explain the spiral arms in gaseous and collisionless self-gravitating disks using the classical non-axisymmetric density perturbations initially proposed for galaxies (Lin & Shu 1964). More recently, other works using hydrodynamical simulations have generated spiral arms through the presence of a massive companion (Kley & Nelson 2012; Zhu et al. 2015). For example, Zhu et al. (2015) found that depending on the mass of the planet, the arms in the circumstellar disks could become more open with a more massive perturber. There are also some works that propose the spiral arms as gravitational instabilities; see Lodato & Rice (2004). However, in those works, the number of spiral arms is larger than those observed in disks.

UX Tauri is a quadruple T Tauri star system located in the Taurus molecular cloud at a distance of 139 ± 2 pc (Bailer-Jones et al. 2018).[7] The system consists of UX Tauri A, the main star, UX Tauri B, separated by 5.''6 to its west, and UX Tauri C, a southern companion only separated by 2.''6 or 360 au (Csépány et al. 2017). UX Tauri B is itself a close binary system

---

[7] However, we found a difference of almost 6 pc between UX Tauri A and C from the GAIA parallaxes (7.15 ± 01 and 6.85 ± 0.1 mas). As we will see, these components should be very close to each other because there is a small difference in the radial velocities between their molecular disks ($\leqslant$1 km s^{-1}) and we were able to resolve the molecular gas that is associated with an interaction. As these components (A and B) are in a binary system, Gaia DR2 possibly did not account for the binary motion when calculating its parallax. The AS 205 system is similar (Kurtovic et al. 2018). Thus, we consider the distance of UX Tauri A and C to be the same for both.

separated by 0.″1 (Correia et al. 2006). The components of the system, UX Tauri A and C, are classified with a spectral type of K2V and M5, stellar masses of $1.3 \pm 0.04\ M_\odot$, and 160 ± 40 Jupiter masses, respectively (Kraus & Hillenbrand 2009). Analysis of the spectral energy distribution (SED) of UX Tauri A suggests the presence of a pre-transitional disk with significant near-infrared excesses, which indicates the presence of an optically thick disk with an inner gap (R_{wall}) of 56 au (Espaillat et al. 2007). Subsequent sensitive Submillimeter Array (SMA) continuum observations at 345 GHz resolved angularly the dusty disk surrounding UX Tauri A with an angular resolution of 0.″3 (Andrews et al. 2011). These submillimeter observations imaged the circumstellar disk inner gap around UX Tauri A and estimated a size of 25 au from the central star (smaller than that estimated by the SED). Near-IR images obtained with the Subaru Telescope revealed a strongly polarized circumstellar disk surrounding UX Tauri A, which extends to 120 au and inclined $46° \pm 2°$ (Tanii et al. 2012).

We note that SMA and Very Large Array (VLA) continuum observations could not detect its companion (UX Tauri C) at a 5σ level, finding 7.5 mJy (0.85 mm) for the SMA (Andrews et al. 2011) and 20 μJy (3.6 cm) for the VLA (Zapata et al. 2017). This companion is only reported in the near-infrared or mid-infrared (Correia et al. 2006; McCabe et al. 2006). At this point, the gas and dust disk associated with UX Tauri C have also not been detected at (sub)millimeter wavelengths (Andrews et al. 2011). One possible reason that the disk is not detected at (sub)millimeter wavelengths is because its circumstellar dusty disk is very faint and small. Neither the dusty nor the gas disk of UX Tauri B have been detected at submillimeter wavelengths.

In this study we present new sensitive and high angular-resolution ($\sim$0.″2–0.″3) archive ALMA CO(2−1)/CO(3−2) observations that reveal a strong interaction between the disks of UX Tauri A and C, separated only by about 360 au. This interaction causes marked spiral arms in the disk UX Tauri A and an extended stream of gas emission in the UX Tauri C disk. These observations additionally reveal for the first time the gas disk and its kinematics in relation to UX Tauri C. Since neither the dusty nor gas disks of UX Tauri B have been detected in these submillimeter ALMA observations, we focus on the A and C components.

2. Observations

2.1. Band 7

The archive observations of UX Tauri were carried out with ALMA on 2016 August 10th and 13th as part of the Cycle 4 program 2015.1.00888.S (PI: Akiyama, Eiji). Part of these data (the 0.87 mm continuum emission) were published in Francis & van der Marel (2020). The observations used 39 (in August 10th) and 37 (August 13th) antennas with a diameter of 12 m, yielding baselines with projected lengths from 15 to 1500 m (18.7–1875 $k\lambda$). The primary beam at this frequency has an FWHM of about 20″, so UX Tauri was covered with a single pointing at the sky position α(J2000) = $04^h30^m3{\overset{s}{.}}99$; δ(J2000) = $+18°13'49{\overset{''}{.}}41$. The integration time on source was about 27 minutes in both sessions.

The weather conditions were very good and stable for these observations, with an average precipitable water vapor between 0.1 and 0.6 mm and an average system temperature around 120 K for August 10th and 150 K for August 13th. The ALMA

calibration included simultaneous observations of the 183 GHz water line with water vapor radiometers used to reduce atmospheric phase fluctuations. The quasars J0510+1800 and J0431+2037 were used for the bandpass, atmosphere, pointing, water vapor radiometer, and flux calibrations. J0431+1731 was used for correcting the gain fluctuations.

The continuum images were obtained by averaging line-free spectral channels of four spectral windows centered at 344.003 GHz(spw0), 355.545 GHz(spw1), 345.809 GHz(spw2), and 356.747 GHz(spw3). The total bandwidth for the continuum is about 4.9 GHz. These four spectral windows were centered to observe different molecular lines: HCO$^+$(4−3) (ν_{rest} = 356.734223 GHz), and ^{12}CO(3−2) (ν_{rest} = 345.795989 GHz). In this study, we concentrated only on the ^{12}CO(3−2) spectral line and the continuum. Each window has a native channel spacing of 488.3 kHz or $\sim$0.41 km s^{-1}.

The data were calibrated, imaged, and analyzed using the Common Astronomy Software Applications (CASA) Version 4.7. Imaging of the calibrated visibilities was done using the CLEAN and TCLEAN tasks. We concatenated the data from both dates with the CONCAT task. We set the robust parameter of CLEAN in CASA to natural for the CO and 0.5 for the continuum image. The resulting image rms noise for the continuum was 40 μJy beam^{-1} at an angular resolution of 0.″18$\times$ 0.″16 with a PA of $-30°$. The ALMA theoretical rms noise for this configuration, integration time, and frequency is about 35 μJy beam^{-1}, which is also very close to the value we obtained in the continuum images. For the line image rms noise we obtained a value of 4.7 mJy beam^{-1} km s^{-1} at an angular resolution of 0.″23 $\times$ 0.″18 with a PA of $-24{\overset{\circ}{.}}6$. The ALMA theoretical rms noise for this configuration, integration time, bandwidth (channel spacing), and frequency are about 4.3 mJy beam^{-1}, which is also very close to the value we obtain in the line images. Phase self-calibration was done in the continuum images and some improvement was obtained. We then applied the solutions to the line maps, obtaining a significant improvement in the channel maps. The thermal emission from the CO can be seen in Figures 1, 3, and 4.

2.2. Band 6

The archival observations of UX Tauri were carried out with ALMA in 2015 August 12th as part of the Cycle 2 program 2013.1.00498.S (PI: Pérez, Laura). Part of these data (the 1.3 mm continuum emission) were published in Pinilla et al. (2018) and Francis & van der Marel (2020). The observations used 44 antennas with a diameter of 12 m, yielding baselines with projected lengths from 15 to 1574 m (11.5–1210 $k\lambda$). The primary beam at this frequency has an FWHM of about 30″, so UX Tauri was covered with a single pointing at the sky position α(J2000) = $04^h 30^m 4{\overset{s}{.}}00$; $\delta(J2000)$ = $+18°13'49{\overset{''}{.}}20$. The integration time on source was about 14.7 minutes.

The quasars J0423−0120, J0510+180, and J0431+2037 were used for the bandpass, atmosphere, pointing, water vapor radiometer, and flux calibration. J0431+2037 was used for correcting the gain fluctuations.

The continuum images were obtained by averaging line-free spectral channels of eight spectral windows. The total bandwidth for the continuum is about 6.3 GHz. These eight spectral windows were centered to observe different molecular lines as for example the ^{13}CO(2−1) (ν_{rest} = 220.3986 GHz), and ^{12}CO(2−1) (ν_{rest} = 230.5380 GHz). Each window has a native channel spacing of
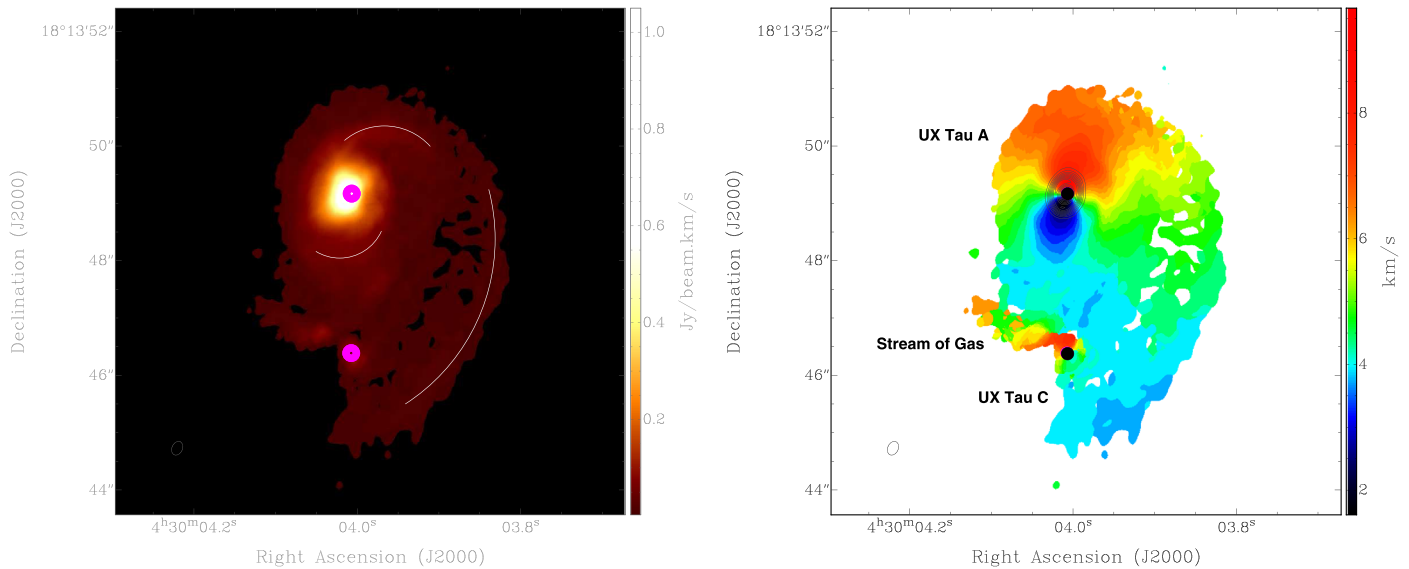
Figure 1. ALMA CO(3−2) moment zero (left) and one (right) images from UX Tauri A and C star system. In the right image (the moment one), we have additionally overlaid in gray contours the continuum 0.85 mm emission from UX Tauri A. We do not detect continuum emission associated with UX Tauri C. The contours range from 10% to 90% of the peak emission, in steps of 10%. The peak of the millimeter continuum emission is 25 mJy beam^{-1}. The half-power contour of the synthesized beam of the line image is shown in the bottom left corner. We integrated in radial velocities from −3.8 to +13.8 km s^{-1} for the CO gas disks in UX Tauri. The LSR systemic velocity of the UX Tauri system is about +5.1 km s^{-1}. The black and magenta circles trace the position of the optical stars reported by the GAIA DR2 data obtained from the SIMBAD database, and we have additionally corrected by the proper motions for both sources. The scale bars in the right represent the intensity (left image) and the radial velocities (right image). The white lines on the right image mark the most evident spiral arms. The position of the component UX Tauri B is outside of this figure.

488.3 kHz or ∼0.61 km s^{-1}. In this study, we concentrated only on the ^{12}CO(2−1) spectral line and the continuum.

The data were calibrated, imaged, and analyzed using the CASA Version 4.4. Imaging of the calibrated visibilities was done using the CLEAN and TCLEAN tasks. We set the `robust` parameter of CLEAN in CASA to `Briggs = 2.0` for the CO and the continuum images. The resulting image rms noise for the continuum was 46 μJy beam^{-1} at an angular resolution of 0″30 × 0″24 with a PA of +9°. The ALMA theoretical rms noise for this configuration, integration time, bandwidth, and frequency is about 34 μJy beam^{-1}, which is very close to the value we obtain in the continuum images. For the line image rms noise we obtained a value of 3.2 mJy beam^{-1} km s^{-1} at an angular resolution of 0″29 × 0″24 with a PA of +8°.2. The ALMA theoretical rms noise for this configuration, integration time, bandwidth (channel spacing), and frequency is about 3.0 mJy beam^{-1}, which is very close to the value we obtain in the line images. Phase self-calibration was done in the continuum images, again obtaining a significant improvement in the channel maps. The thermal emission from the CO can be seen in Figures 2 and 5.

3. Results and Discussion

3.1. UX Tauri System (A/C)

In Figures 1 and 2 we present the main results of this ALMA study. In Figure 1, the moment zero (integrated intensity) and one (intensity-weighted velocity) maps of the CO(3−2) thermal emission are presented. In addition to these maps, we have overlaid in contours the 0.85 mm continuum emission together with the moment one map, and the positions of the optical stars related to UX Tauri A and C obtained with the GAIA DR2 data and corrected by the proper motions obtained from this catalog (Gaia Collaboration et al. 2018); see Figure 1. The continuum images are very similar to those presented in Pinilla et al. (2018) and Francis & van der Marel (2020).

The high fidelity and sensitive CO images of the UX Tauri A/C system presented here reveal for the first time the gas structure of the disks. Recent ALMA images of UX Tauri A/C could not reveal this structure and only imaged the molecular emission very close to the UX Tauri A disk; see Figure 4 from Akeson et al. (2019). The line rms noise obtained for the CO(2−1) in Akeson et al. (2019), however, was very high (39 mJy beam^{-1} km s^{-1}) compared with our observations (3.2 mJy beam^{-1} km s^{-1}). On the other hand, our maps reveal for the first time marked molecular gas spiral arms connecting the UX Tauri A/C system. These arms seem to arise from the north side of UX Tauri A and go directly to the south, where its companion C is localized. Futhermore, there are two thin and bright (with an angular size of only about 1″) spiral arms close to UX Tauri A; one begins in the north part of the disk and extends to the west, and the other one starts in the south and extends to the east (see Figure 1). Very close to the innermost part of the UX Tauri A disk, where the continuum emission is located, the CO emission is probably optically thick, and not much structure is observed. This physical opacity effect has already been observed in other disks as, e.g., IRAS16293 (Zapata et al. 2013), at higher frequencies and HL Tau (ALMA Partnership et al. 2015).

In Figure 1, as mentioned before, we include a map of the CO(3−2) moment one emission from the UX Tauri system. In order to compute this map, we integrated in radial velocities from −3.8 to +13.8 km s^{-1} for the CO gas disks in UX Tauri. The LSR systemic velocity of the UX Tauri system is about +5.1 km s^{-1} (Akeson et al. 2019). From this image, we can see clearly the two rotating disks associated with UX Tauri A and C. In both disks the redshifted velocities are found to the north and the blueshifted ones are toward the south. There is one extra tail that seems to connect the redshifted part of the rotating disk associated with UX Tauri C. The redshifted velocities begin from the UX Tauri C disk and go to the east, with a pattern clearly different from the Keplerian behavior of the gas in the UX Tauri A disk. This is the first time
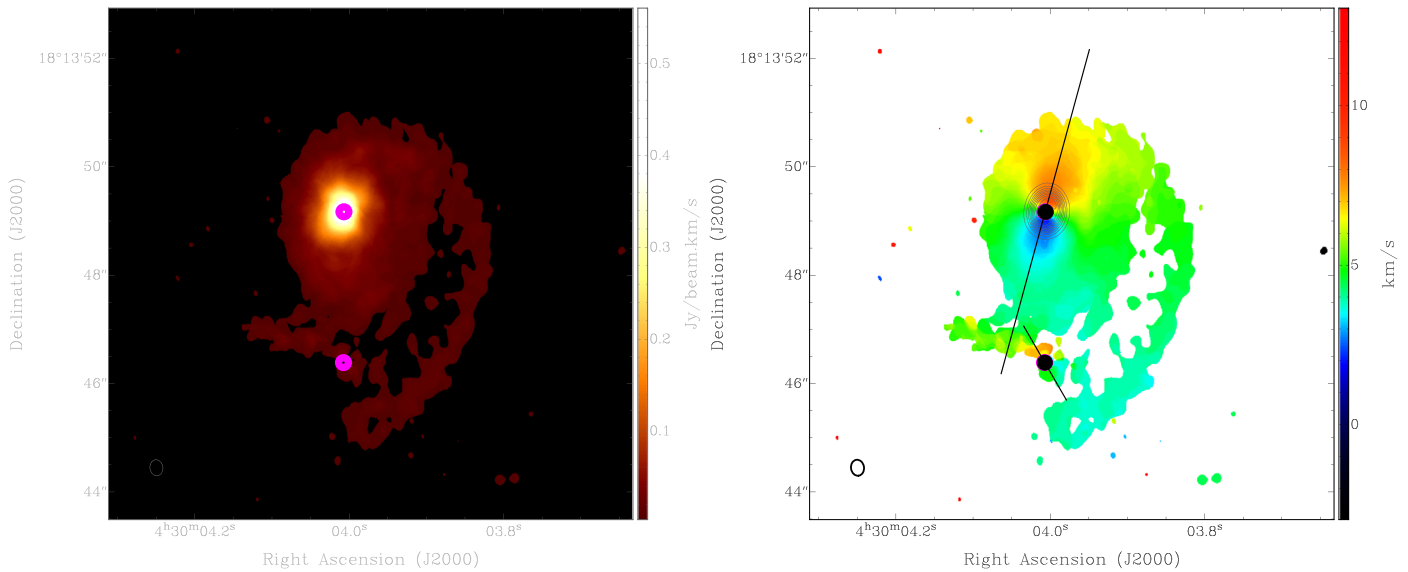
Figure 2. ALMA CO(2−1) moment zero (left) and one (right) images from UX Tauri A and C star system. In the right image (the moment one), we have additionally overlaid in gray contours the continuum 1.3 mm emission from UX Tauri A. We do not detect continuum emission associated with UX Tauri C. The contours range from 10% to 90% of the peak emission, in steps of 10%. The peak of the millimeter continuum emission is 15 mJy beam^{-1}. The half-power contour of the synthesized beam of the line image is shown in the bottom left corner. We integrated in radial velocities from −3.8 to +13.8 km s^{-1} for the CO gas disks in UX Tauri. The LSR systemic velocity of the UX Tauri system is about +5.1 km s^{-1}. The black and magenta circles trace the position of the optical stars reported by the GAIA DR2 data obtained from the SIMBAD database, we have additionally corrected by the proper motions for both sources, similar to Figure 1. The scale bars in the right represent the intensity (left image) and the radial velocities (right image). The blue (UX Tauri A) and red (UX Tauri C) lines trace the position where the position–velocity diagrams shown in Figures 4 and 5 were computed. The position of the component UX Tauri B is outside of this figure.

that this disk and the tail have been reported. The kinematics of the gas revealed in Figure 1 show that the radial velocities of the spiral tails in this system follow the same structure as the disk in UX Tauri A, which suggests that these tails are likely disrupted molecular material from UX Tauri A's surroundings.

From Figure 1, we can obtain the positions and structure of the disks. For the UX Tauri A CO molecular disk, we obtained from our model a deconvolved size of 1800 mas with a position angle (PA) of 164° ± 8°. For the disk in UX Tauri C, it is more difficult to obtain a deconvolved size and a PA because there is a large amount of intervening gas from the eastern tail and the UX Tauri A spiral arms. However, from Figure 1 we estimated roughly a size of <400 mas and a PA of 30°. We should be cautious with these numbers obtained for the component C because they are upper limits. As the position angles are different for both disks, this suggests that maybe the disks are not coplanar (or are not rotating in the same plane) and the eastern molecular tails are also in a different plane.

For the continuum emission, our image reveals the pre-transitional disk reported for UX Tauri A and already mapped at these wavelengths by the SMA and ALMA (Andrews et al. 2011; Akeson et al. 2019), as was mentioned earlier. Our continuum 0.85 mm map has a structure similar to those of these observations, e.g., the inner cavity. We do not detect the UX Tauri C component at the 5σ level (0.2 mJy beam^{-1}). From a Gaussian fitting to the 0.85 mm continuum emission from UX Tauri A, we obtained a deconvolved size of 570 ± 30 × 420 ± 30 mas^2 with a PA of 167° ± 9° and an integrated flux of 197 ± 12 mJy.

Figure 2 is similar to Figure 1, but with the line CO(2−1) detected at band 6. Here, we have additionally included the 1.3 mm continuum emission from the UX Tauri A/C system. The thermal CO(2−1) and 1.3 mm continuum emission show a very similar structure to that revealed in the CO(3−2) and 0.85 mm images, as shown in Figure 1. This figure confirms the marked molecular gas spiral arms connecting the UX Tauri

A/C system, and the two rotating disks associated with UX Tauri A and C. These rotating disks have similar characteristics as revealed in the CO(3−2) maps. From both figures, the CO molecular emission from the disk of UX Tauri A has an extent of about 3″ × 2″ or 420 au × 280 au, quite large compared to the (sub)millimeter continuum disk (a factor of >5). Even if comparing this difference in size between the continuum and the molecular emission in other transitional disks (e.g., SR24S (∼1); 2MASS J16042165-213028 (∼2); DM Tauri (∼1); T Chamaeleontis (∼2); Huélamo et al. 2015; Fernández-López et al. 2017; Kudo et al. 2018; Mayama et al. 2018; van Terwisga et al. 2019), this difference is still quite large for UX Tauri A. However, Facchini et al. (2019) reported in CX Tauri a large difference in the millimeter dust and gas extents (>5) and argued that this could be explained due by a radial drift, which closely matches the predictions of theoretical models. This difference in dust and gas extents is well known for UX Tauri A; however, it is not clear for UX Tau C because we did not detect the continuum emission.

Figure 3 presents the channel spectral maps of the CO(3−2) emission from the UX Tauri A/C system. The channel maps from the CO(2−1) emission are similar and are not presented here. Together with this CO(3−2) channel map we have computed a Keplerian thin-disk model fitted to the line data from UX Tauri A and overlaid it in this channel map. As the emission from UX Tauri C is very contaminated by the disk interaction between both components, a Keplerian thin-disk model could not be obtained. Pinte et al. (2018) demonstrated that neglecting the vertical structure of the disk (assuming a thin disk) has a small impact on the derived stellar mass, especially in CO lines. Thus, the dynamical mass and other parameters obtained with this simple model constrain the disk structure.

The best physical parameters of the Keplerian disk surrounding UX Tauri A are presented in Table 1. This Keplerian thin-disk
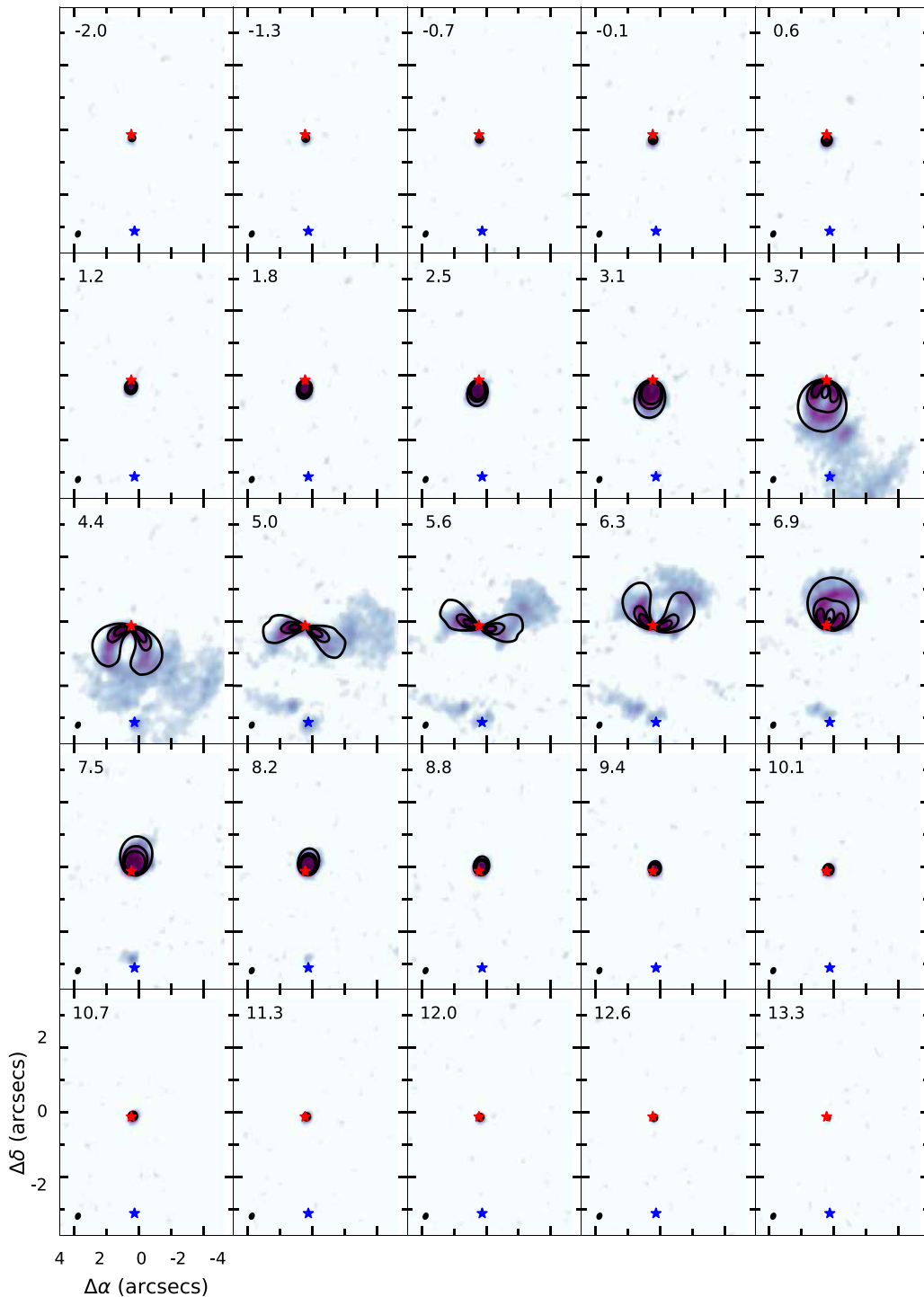
Figure 3. ALMA CO(3−2) channel velocity maps overlaid with our best synthetic model of a Keplerian thin disk in the black contours of UX Tauri A. The contours are in units of percent of the peak emission. The red and blue stars mark the position of the optical stars associated with UX Tauri A and UX Tauri C, respectively. The radial velocity corresponding to each channel bin is shown in the upper left corner and is in km s^{-1}. Every channel map is centered on UX Tauri A. Here, we smoothed our channel spacing to 0.7 km s^{-1} to obtain a better sensitivity. The position (0, 0) corresponds to the position of UX Tauri A.

model is described in detail in Appendix B of Zapata et al. (2019) and we will not discuss this again here. From Figure 3, we note that there is good correlation between the channel map emission from the disk of UX Tauri A and the best Keplerian thin-disk model fit. Residual maps from the model and observations can be obtained; however, there is a large amount of intervening emission that gets bright in the residual, thus we are not presenting these maps here. From this disk model, we obtained three important

parameters with a good precision, the inclination angle $i = 32° \pm 8°$, the size $1″8 \pm 0″3$ (250 au), and the enclosed mass (disk+star) $1.4 \pm 0.6\,M_\odot$. The compact gas disk from UX Tauri C and the redshifted molecular gas bridge can also be seen in the southern part of the channel maps.

Figures 4 and 5 reveal the kinematics of the molecular gas within both disks, UX Tauri A/C. In these Figures, we present the position–velocity (PV) diagrams obtained along the major

Table 1
Physical Parameters from the Best Keplerian Thin-disk Fit for UX Tauri A

Physical Parameter	Estimated Value from the Model
Line-width (Δv)	1.6 ± 0.2 km s^{-1}
Beam-width (Δs)	$0\rlap{.}''21$ (fixed)
Central velocity of the Disk (v_0)	$+5.1 \pm 0.1$ km s^{-1}
Inclination Angle (i)	$32° \pm 8°$
Inner Disk Radius (r_1)	$0\rlap{.}''01$(fixed)
Outer Disk Radius (r_2)	$1\rlap{.}''8 \pm 0\rlap{.}''3$
Infall Velocity (v_i at r_0)	-0.1 ± 0.2 km s^{-1}
Rotational Velocity (v_r at r_0)	$+4.5 \pm 1.0$ km s^{-1}
Reference Radius (r_0)	$0\rlap{.}''5$ (70 au)
Enclosed Mass (star+gas)	$1.4 \pm 0.6\ M_\odot$

axis of both disks. In the PV diagram of the disk of UX Tauri A (Figure 4), we have additionally overlaid the PV diagram from the thin-disk model obtained in this paper. Both PV diagrams have good correspondence, rendering clearly and with good fidelity the Keplerian curves. For the case of UX Tauri C, we could not obtain a model, so we only plotted the rotational Keplerian curves of enclosed masses (disk+star) of 100, 70, and 40 Jupiter masses. Therefore, we consider UX Tauri C could have an enclosed mass of $70 \pm 30/\sin i$ (where i is the inclination) Jupiter masses, straddling the line between a brown dwarf and a low-mass star. Here, we did not correct the mass for the inclination of the disk because the gas emission from the disk is very contaminated. ALMA observations with a better angular resolution might help with better tracing the disk and thus its inclination angle. The physical size of this gas disk is < 56 au, as mentioned earlier. As this gas disk is first reported here, these parameters cannot be compared; however, we note that the mass of the star obtained from the optical is 160 Jupiter masses (Kraus & Hillenbrand 2009). More recent estimations, however, reported a mass for UX Tauri C of 87 Jupiter masses (Csépány et al. 2017), which is very similar to that given here. These masses, however, were obtained from the stellar models, contrary to our values that were obtained from the ALMA CO observations.

Molecular disks have been detected toward a handful of low-mass or substellar objects. Some examples are IC 348-SMM2E (Palau et al. 2014), TWA 34 (Rodriguez et al. 2015), Rho Oph 102 (Ricci et al. 2012), and 2MASS J04442713+2512164 (Ricci et al. 2014). However, none of these disks seem to be associated with a multiple system like UX Tauri.

3.2. Dust and Gas Mass

The position angle is in good agreement with the one obtained for CO(3–2) (see above). The corresponding physical sizes of these deconvolved values are about 70 au, which suggest we are only seeing the circumstellar disk, and at the 5σ level (0.175 mJy Beam^{-1}) no dust emission arises from the spirals measured in CO emission. Assuming that the dust emission is optically thin and isothermal, the dust mass (M_d) is directly proportional to the flux density (S_ν) integrated over the source as

$$M_d = \frac{D^2 S_\nu}{\kappa_\nu B_\nu(T_d)}, \qquad (1)$$

where D is the distance to UX Tauri A (139 pc, Bailer-Jones et al. 2018), κ_ν is the dust mass opacity, and $B_\nu(T_d)$ is the Planck function for the dust temperature T_d. In reality, the
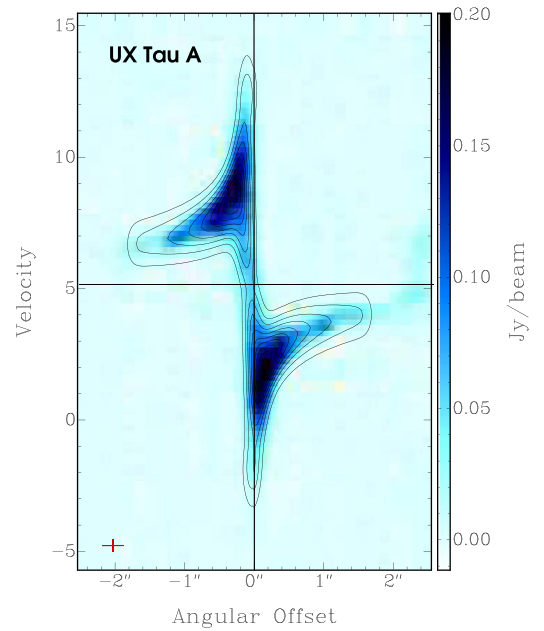

Figure 4. PV diagram computed along the major axis of the circumstellar disk of UX Tauri A (PA = 164°). The blue scale image is obtained from the ALMA CO(3–2) data and the contour image is from our synthetic model. The contours range from 10% to 90% of the peak emission, in steps of 10%. The peak of the millimeter continuum emission is 0.2 Jy beam^{-1}. The spectral and angular resolutions are shown in the bottom left corner. The black lines mark the systemic cloud velocity ($+5.1$ km s^{-1}) and the disk axis center. The scale bar on the right represents the intensity.
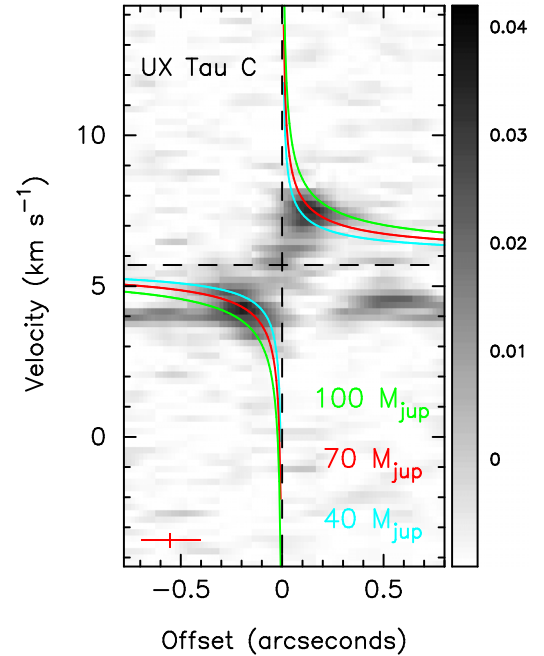

Figure 5. PV diagram computed along the major axis of the circumstellar disk of UX Tauri C (PA = 30°). The grayscale image is obtained from the ALMA CO(3–2) data. The spectral and angular resolutions are shown in the bottom left corner. The dashed lines mark the systemic cloud velocity ($+5.8$ km s^{-1}) and the disk axis center. The scale bar on the right represents the intensity and is units of Jy beam^{-1}. The cyan, red, and green lines mark the Keplerian rotation curves for a disk with enclosed masses (disk+star) of 100 (white), 70 (red), and 40 (green) Jupiter masses, respectively.

thermal dust emission is probably not optically thin, hence the estimated mass is considered to be a lower limit. Assuming a dust mass opacity (κ_ν) of 0.025 cm^2 g^{-1} (of dust+gas, and

taking a gas-to-dust ratio of 100) appropriate for these wavelengths (1.3 mm) (Ossenkopf & Henning 1994), as well as a characteristic dust temperature of 50 K, we estimated a lower limit for the mass (dust+gas) of the disk associated with UX Tauri A of 0.005 $M_\odot$. The mass uncertainty could be very large (a factor of up to 3 or 4) given the uncertainty in the opacity and in the dust temperature. This mass estimation is in good agreement with the value estimated by Andrews et al. (2011). For the component UX Tauri C, we can estimate an upper limit for its total dust mass. Taking a dust temperature of 20 K, because this is a young star with a low mass, a flux density of 0.2 mJy, and a dust mass opacity similar to that of UX Tauri A, we found a dust mass for UX Tauri C of $\leqslant 0.05$ $M_\oplus$. As we do not detect gas emission, we only are considering the dust mass for this component. This total dust mass could be associated with the disk of UX Tauri C. A similar upper limit can be considered for the component UX Tauri B.

3.3. UX Tau B

We did not detect continuum or line emission from the companion UX Tauri B in both bands, localized to the west, above a 4σ threshold (200 μJy beam^{-1} for the continuum at 0.85 mm, and 12.8 mJy beam^{-1} km s^{-1} for the CO(3–2) line). The disk of UX Tau B falls outside of the images and is thus not indicated.

3.4. UX Tauri C: A Possible Low-mass Object Flyby

The ALMA CO molecular observations toward the UX Tauri system clearly reveal the tidal interaction between the components of the UX Tauri A/C system, exhibiting pronounced spiral arms. This type of physical interaction in young triple- and higher-order multiple stellar systems was discussed in Reipurth et al. (2014). Moreover, this scenario was debated by Csépány et al. (2017) for this system, who analyzed multi-epoch high-spatial resolution observations in the optical and NIR bands in UX Tauri and concluded that despite UX Tauri A and B probably being gravitationally bound, the status of the UX Tauri A and C system is not entirely clear. However, since the semimajor axis of the orbit between UX Tauri A and C is significantly affected by the estimation of the inclination, they could not confirm the classification of UX Tau A/C as an unstable triple system.

We propose that UX Tauri C is perhaps experiencing a flyby due to a close-by dynamical interaction with the component UX Tau A. It is likely that this flyby is not a one-time flyby by a completely unaffiliated random young brown dwarf in a similar evolutionary state that happens to be free-floating in the sparse Taurus association. Therefore, UX Tau C could be experiencing the closest approach of a wide, evolving, and eccentric orbit for the first time in thousands of years.

Here, we mention some characteristics from our new ALMA observations of the system supporting this flyby scenario:

1. The two CO disks are probably neither coplanar nor aligned.
2. The CO extended gas shows spiral arms and a bridge linking the A and C disks. These features are predicted by simulations of prograde close encounters or flybys (e.g., Vorobyov et al. 2017; Cuello et al. 2019, 2020).

3. The spiral arms in UX Tauri A disk have pitch angles between 20° and 30°. These large values do not agree with the spiral patterns produced by gravitational fragmentation of disks, which are typically more roundish, with pitch angles ranging from 10° to 20° (Cuello et al. 2019, 2020). The pitch angles of the disk interactions seem to be small, as seen in the case of AS 205 (14°; Kurtovic et al. 2018) or for HT Lup A (4°; Kurtovic et al. 2018).
4. The kinematics of the CO tail extending due east of the disk of UX Tauri C are compatible with a structure non-coplanar with the UX Tauri A disk. It is at a more redshifted radial velocity than the gas from the south part of the UX Tauri A disk. It shows a velocity gradient from west (blue) to east (red), bridging some of the southwest part of the UX Tauri A disk with the redshifted part of the UX Tauri C disk. Hence, this CO bridge could be interpreted as a loop of gas in the foreground of the UX Tauri A disk, rising from this disk and infalling into the UX Tauri C disk. These kind of loop structures are produced in simulated encounters between a disk and a prograde perturber with a trajectory inclined with respect to the plane of the main disk (e.g., Figures 4 and 5; for a flyby with an inclination of 45° see Cuello et al. 2019, 2020).
5. UX Tauri C has a gas disk. Simulations of prograde flybys also predict that the perturber strips gas from the main disk (Vorobyov et al. 2017; Cuello et al. 2019, 2020).
6. The UX Tauri A disk presents a large central cavity. In addition to the truncation of the disks a flyby can also produce wide inner cavities through tidal interactions at the core of the perturbed disks, as shown again in the recent flyby simulations by Cuello et al. (2019, 2020).

There could exist other possible scenarios to generate spiral arms in a disk, but they are not as favorable as the flyby described above. Either disk fragmentation due to gravitational instabilities, perturbations by a planet or a stellar embedded companion, or a massive external body via gravity or asymmetric illumination induce the formation of spiral arms in a disk. However, a disk fragmentation is not favorable in disks with small masses, like the one around UX Tauri A. We can make a rough estimate of the Toomre Q parameter, which for Keplerian disks is approximately

$$Q \simeq 2(M_*/M_{\rm disk}) \cdot (H/R_{\rm disk}), \qquad (2)$$

where M_* and $M_{\rm disk}$ are the mass of the star and the disk respectively, H is its scale height, and $R_{\rm disk}$ is its outer radius. Assuming a low average disk temperature of 50 K (hence a sound speed $c_s = 0.6$ km s^{-1}), an angular velocity $\Omega = 4 \times 10^{-10}$ km s^{-1} (derived using the values of v at r_0 from Table 1), an outer disk radius of 252 au (Table 2) and derived disk and stellar masses (0.007 $M_\odot$ and 1.4 $M_\odot$, respectively), we obtain a $Q = 11$, which is well over unity, implying that UX Tauri A is a stable disk against gravitational disturbances. An embedded companion in the disk typically displays a spiral pattern with a smaller pitch angle and a more symmetric pattern, with equal spirals on both sides of the disk. An external perturber (farther out than UX Tau C) is also ruled out, since UX Tauri B is probably neither massive nor luminous enough to induce the spirals

displayed by the disk. It is important to note that the spiral arms connect directly to UX Tau C, ruling out UX Tau B as a perturber.

One can estimate whether UX Tauri C is bounded to UX Tauri A's gravitational field. From Figure 5 in Csépány et al. (2017), we estimated a tangential velocity of $0\rlap{.}''1$ per 27.5 yr or $2.4 \pm 0.5\,\mathrm{km\,s^{-1}}$. This motion comes mainly from the decl., as the motion in R.A. is null. From the PV diagrams shown in Figures 4 and 5 we roughly estimated a radial velocity for UX Tauri C of about $0.7 \pm 0.3\,\mathrm{km\,s^{-1}}$. Thus, the total velocity is $\sim 2.5 \pm 0.6\,\mathrm{km\,s^{-1}}$. For a body orbiting a star with a mass of UX Tauri A ($1.3\,M_\odot$) at a distance of 360 au and in a circular orbit, an orbital velocity of less than $1.8\,\mathrm{km\,s^{-1}}$ is needed to be bound. As the UX Tauri C velocity is a bit larger, this may indicate that this object is unbound to the gravitational field of UX Tauri A, but if we take into account the uncertainties on the total velocity, it still is not very clear. Furthermore, if we take a parabolic orbit (which is expected from a periastron passage in a dynamically evolving eccentric and wide orbit), the orbital velocity increases by a factor of $\sqrt{2}$, so this might indicate that it is still bound.

All of the observational evidence presented here led us to propose that UX Tauri C is passing in a prograde flyby close to the disk of UX Tauri A. The former UX Tauri C, coming from the background, has probably captured some gas from the UX Tauri A disk and it is forming a new disk that is already orbiting it. The tidal interaction has caused the formation of spiral arms, one of which is rotating in the plane of the main disk and the other inclined toward the foreground, bridging both young stars.

The case presented here is therefore one of a few cases (HD 100453 AB, AS 205, SU Aurigae, RW Aurigae) of binary disk interactions mapped in molecular gas (Dai et al. 2015; Kurtovic et al. 2018; Akiyama et al. 2019; van der Plas et al. 2019). AS 205 and RW Aurigae are considered tidal encounters with parabolic orbits or flybys. However, the intruder does not have a substellar mass in any of them, so this is the first time that it has been reported. These two examples revealed molecular gas bridges between the disks and the stream-like structures extending from the main component. Depending on whether or not the encounter is prograde or retrograde the material transferred from one circumstellar disk to another is more pronounced (Dai et al. 2015). As mentioned before we think that the encounter in UX Tauri A/C could be prograde, as suggested for the AS 205 object.

4. Conclusions

In this study, we present sensitive and high angular-resolution ($\sim 0\rlap{.}''2$–$0\rlap{.}''3$) (sub)millimeter (230 and 345 GHz) continuum and $CO(2-1)/CO(3-2)$ line observations of the UX Tauri A/C disk system located in the Taurus molecular cloud using ALMA. The main results of our work can be summarized as follows:

1. These observations reveal the gas and dusty disks surrounding the young star UX Tauri A with great detail, and for the first time we have detected the molecular gas emission associated with the disk of UX Tauri C (with a size of ~ 56 au). No (sub)millimeter continuum emission is detected at the 5σ level (0.2 mJy at 0.85 mm) associated with UX Tauri C in both bands.

2. We report a strong tidal disk interaction between both disks, UX Tauri A/C, separated (at a projected distance) by only 360 au. The CO line observations revealed marked spiral arms in the disk of UX Tauri A and an extended redshifted stream of gas associated with the UX Tauri C disk. We discuss the possibility of UX Tauri C being a young brown dwarf dwarf flyby given all the observational constraints.

3. The enclosed mass (disk+star) estimation from the disk Keplerian radial velocities are $1.4 \pm 0.6\,M_\odot$ for UX Tauri A, and $70 \pm 30/\sin i$ Jupiter masses for UX Tauri C. For the component UX Tauri C, we can estimate a dust mass in its disk of $\leqslant 0.05\,M_\oplus$.

Facility: ALMA .

Software: CASA(McMullin et al. 2007), KARMA(Gooch 1996).

ORCID iDs

Luis A. Zapata ⓘ https://orcid.org/0000-0003-2343-7937
Luis F. Rodríguez ⓘ https://orcid.org/0000-0003-2737-5681
Aina Palau ⓘ https://orcid.org/0000-0002-9569-9234
Robert Estalella ⓘ https://orcid.org/0000-0001-7341-8641
Mayra Osorio ⓘ https://orcid.org/0000-0002-6737-5267
Guillem Anglada ⓘ https://orcid.org/0000-0002-7506-5429
Nuria Huelamo ⓘ https://orcid.org/0000-0002-2711-8143

References

Adams, F. C., Ruden, S. P., & Shu, F. H. 1989, ApJ, 347, 959
Akeson, R. L., Jensen, E. L. N., Carpenter, J., et al. 2019, ApJ, 872, 158
Akiyama, E., Vorobyov, E. I., Baobabu Liu, H., et al. 2019, AJ, 157, 165
ALMA Partnership, Brogan, C. L., Pérez, L. M., et al. 2015, ApJL, 808, L3
Andrews, S. M., Wilner, D. J., Espaillat, C., et al. 2011, ApJ, 732, 42
Ansdell, M., Williams, J. P., Manara, C. F., et al. 2017, AJ, 153, 240
Bailer-Jones, C. A. L., Rybizki, J., Fouesneau, M., et al. 2018, AJ, 156, 58
Bally, J., O'Dell, C. R., & McCaughrean, M. J. 2000, AJ, 119, 2919
Bate, M. R. 2018, MNRAS, 475, 5618
Correia, S., Zinnecker, H., Ratzka, T., et al. 2006, A&A, 459, 909
Csépány, G., van den Ancker, M., Ábrahám, P., et al. 2017, A&A, 603, A74
Csépány, G., van den Ancker, M., Ábrahám, P., et al. 2017, A&A, 603, A74
Cuello, N., Dipierro, G., Mentiplay, D., et al. 2019, MNRAS, 483, 4114
Cuello, N., Louvet, F., Mentiplay, D., et al. 2020, MNRAS, 491, 504
Dai, F., Facchini, S., Clarke, C. J., et al. 2015, MNRAS, 449, 1996
Duchêne, G., & Kraus, A. 2013, ARA&A, 51, 269
Espaillat, C., Calvet, N., D'Alessio, P., et al. 2007, ApJL, 670, L135
Facchini, S., van Dishoeck, E. F., Manara, C. F., et al. 2019, A&A, 626, L2
Fernández-López, M., Zapata, L. A., & Gabbasov, R. 2017, ApJ, 845, 10
Francis, L., & van der Marel, N. 2020, ApJ, 892, 111

Gooch, R. 1996, in ASP Conf. Ser. 101, Astronomical Data Analysis Software and Systems V, ed. G. H. Jacoby & J. Barnes (San Francisco, CA: ASP), 80

Gaia Collaboration, Brown, A. G. A., Vallenari, A., et al. 2018, A&A, 616, A1

Huang, J., Andrews, S. M., Dullemond, C. P., et al. 2018, ApJL, 869, L42

Huélamo, N., de Gregorio-Monsalvo, I., Macias, E., et al. 2015, A&A, 575, L5

Kley, W., & Nelson, R. P. 2012, ARA&A, 50, 211

Kraus, A. L., & Hillenbrand, L. A. 2009, ApJ, 704, 531

Kudo, T., Hashimoto, J., Muto, T., et al. 2018, ApJL, 868, L5

Kurtovic, N. T., Pérez, L. M., Benisty, M., et al. 2018, ApJL, 869, L44

Laughlin, G., & Korchagin, V. 1996, ApJ, 460, 855

Lin, C. C., & Shu, F. H. 1964, ApJ, 140, 646

Lodato, G., & Rice, W. K. M. 2004, MNRAS, 351, 630

Mayama, S., Akiyama, E., Panić, O., et al. 2018, ApJL, 868, L3

McCabe, C., Ghez, A. M., Prato, L., et al. 2006, ApJ, 636, 932

McMullin, J. P., Waters, B., Schiebel, D., Young, W., & Golap, K. 2007, in ASP Conf. Ser. 376, Astronomical Data Analysis Software and Systems XVI, ed. R. A. Shaw, F. Hill, & D. J. Bell (San Francisco, CA: ASP), 127

O'Dell, C. R., Muench, A., Smith, N., et al. 2008, in Handbook of Star forming Regions, Volume I: The Northern Sky, Vol. 4, ed. B. Reipurth (San Francisco, CA: ASP), 544

Osorio, M., Macías, E., Anglada, G., et al. 2016, ApJL, 825, L10

Ossenkopf, V., & Henning, T. 1994, A&A, 291, 943

Palau, A., Zapata, L. A., Rodríguez, L. F., et al. 2014, MNRAS, 444, 833

Pinilla, P., Tazzari, M., Pascucci, I., et al. 2018, ApJ, 859, 32

Pinte, C., Ménard, F., Duchêne, G., et al. 2018, A&A, 609, A47

Reipurth, B., Clarke, C. J., Boss, A. P., et al. 2014, in Protostars and Planets VI, ed. H. Beuther et al. (Tucson, AZ: Univ. Arizona Press), 267

Ricci, L., Testi, L., Natta, A., et al. 2012, ApJL, 761, L20

Ricci, L., Testi, L., Natta, A., et al. 2014, ApJ, 791, 20

Rodriguez, D. R., van der Plas, G., Kastner, J. H., et al. 2015, A&A, 582, L5

Ruíz-Rodríguez, D., Cieza, L. A., Williams, J. P., et al. 2018, MNRAS, 478, 3674

Tanii, R., Itoh, Y., Kudo, T., et al. 2012, PASJ, 64, 124

van der Plas, G., Ménard, F., Gonzalez, J.-F., et al. 2019, A&A, 624, A33

van Terwisga, S. E., van Dishoeck, E. F., Cazzoletti, P., et al. 2019, A&A, 623, A150

Vorobyov, E. I., Steinrueck, M. E., Elbakyan, V., et al. 2017, A&A, 608, A107

Williams, J. P., & Cieza, L. A. 2011, ARA&A, 49, 67

Zapata, L. A., Garay, G., Palau, A., et al. 2019, ApJ, 872, 176

Zapata, L. A., Loinard, L., Rodríguez, L. F., et al. 2013, ApJL, 764, L14

Zapata, L. A., Rodríguez, L. F., & Palau, A. 2017, ApJ, 834, 138

Zhu, Z., Dong, R., Stone, J. M., et al. 2015, ApJ, 813, 88